

## A pseudo-analytical model for CSD spillage due to rotational velocity-induced flow

Werkhoven, Jeroen; Nieuwboer, Bas; Ramsdell, R. C.; Louis, A.A.; Miedema, Sape

**Publication date**

2018

**Document Version**

Final published version

**Published in**

Proceedings of the Dredging Summit and Expo 2018

**Citation (APA)**

Werkhoven, J., Nieuwboer, B., Ramsdell, R. C., Louis, A. A., & Miedema, S. (2018). A pseudo-analytical model for CSD spillage due to rotational velocity-induced flow. In *Proceedings of the Dredging Summit and Expo 2018* (pp. 145-161). Article Paper 4a-1 Western Dredging Association.

**Important note**

To cite this publication, please use the final published version (if applicable). Please check the document version above.

**Copyright**

Other than for strictly personal use, it is not permitted to download, forward or distribute the text or part of it, without the consent of the author(s) and/or copyright holder(s), unless the work is under an open content license such as Creative Commons.

**Takedown policy**

Please contact us and provide details if you believe this document breaches copyrights. We will remove access to the work immediately and investigate your claim.

## A PSEUDO-ANALYTICAL MODEL FOR CSD SPILLAGE DUE TO ROTATIONAL VELOCITY-INDUCED FLOW

J.J. Werkhoven<sup>1</sup>, B.J. Nieuwboer<sup>2</sup>, A.A. Louis<sup>3</sup>, R.C. Ramsdell<sup>4</sup>, S.A. Miedema<sup>5</sup>

### ABSTRACT

This paper proposes a classification of the concurrent sources of Cutter Suction Dredger (CSD) spillage as well as a pseudo-analytical model for a-priori computation of spillage rates due to high rotational velocity-induced flow. As of yet, in literature, no analytical models exist that describe spillage due to centrifugal advection. Based on work performed by Miedema (2017) and Nieuwboer (2018), a preliminary model is set up that includes most relevant cutting variables, or a simplification thereof. However, in this preliminary model, the axial pump effect described in Den Burger is not explicitly accounted for and the pressures exerted on the cutterhead contour are heavily simplified. An adaptation of a governing dimensionless velocity ratio proposed by Steinbusch et al. (1999) and Dekker et al. (2003) is used for model calibration using experimental data for sand from Miltenburg (1983) and rock from Den Burger (2003). Model parameters were identified for which sand spillage can be estimated within a 5 percentage point bandwidth of the experimental data. Moreover, the shape of the model plot appears to resemble that of the data for sand accurately, i.e. the model behaves as expected. The preliminary model is not capable of accurately estimating rock spillage rates over a wide range of mixture velocities. This inaccuracy may be ascribed to the concurrence of other spillage sources. The preliminary proposed model may not entirely capture the centrifugal effect of the cutterhead for larger grain sizes. Recommendations are given for further research.

**Keywords:** Dredging, Spillage, CSD, Centrifugal Advection, Entrainment, Redeposition, Model Calibration

### INTRODUCTION

Depending on its size and installed power, a Cutter Suction Dredge (CSD) is capable of cutting a wide range of soil types from silts and clays to fractured or solid rocks. Its high precision allows for utilization in a variety of dredge operations including navigational channel deepening, port construction and pipeline trenching. In spite of being considered relatively efficient, a CSD can spill significantly. Den Burger (2003) defines spillage as “the soil that is cut during the dredging process, but is not sucked up by the suction pipe”. This paper approaches spillage as perceived by the dredging industry and defines spillage as “any soil that may be dislodged above the lowest cutter tip trajectory, but is not sucked into the suction pipe”. In contrast to Den Burger’s definition, this includes any soil in the vicinity of the cutter and above the cutter profile, but not directly in contact with the cutting equipment.

A CSD is equipped with a rotating cutter head that is mounted in front of a suction mouth. A hoistable ladder carries the installation and along with a set of swing winches, provides sufficient weight and force to laterally maneuver the rotating cutter head through the soil. When the swing velocity and the tangential velocity at the top of the cutter are aligned, a scenario arises that is referred to as “over-cutting” (back swinging), while opposing vectors render an “under-cutting” (dig swinging) scenario. See Figure 1 for a visual representation of these scenarios. Typically, the cutter consists of 5 or 6 blades with a series of teeth that mechanically excavate and suspend bank sediment in order

<sup>1</sup> MSc Student Offshore And Dredging Engineering, Delft University of Technology, Mekelweg 2, 2628 CD, Delft, The Netherlands, T: ++31 -15 27 89111, Email: J.J.Werkhoven@student.tudelft.nl

<sup>2</sup> PhD candidate, Delft University of Technology, Mekelweg 2, 2628 CD, Delft, The Netherlands, T: ++31-15-2789296, Email: B.J.Nieuwboer@tudelft.nl

<sup>3</sup> Cutting Equipment Engineer, IHC Holland B.V., Smitweg 6, 2961AW, Kinderdijk, The Netherlands, T: ++31-88-0152902, Email: aa.louis@royalihc.com

<sup>4</sup> Director of Production Engineering, Great Lakes Dredge & Dock Company, 2122 York Road, Oakbrook, IL, 60523, USA, T: +1 630-574-3463, Email: rcramsdell@gldd.com

<sup>5</sup> Associate Professor, Delft University of Technology, Mekelweg 2, 2628 CD, Delft, The Netherlands, T: ++31-15-2788359, Email: s.a.miedema@tudelft.nl

to be sucked up by the suction mouth. According to Den Burger, spillage can be attributed to the cutting process as well as the mixture forming process.

To compensate for reduced depth due to spillage, CSD operators resort to “overdepth cutting” which entails cutting deeper than theoretically required. Overdepth cutting has a number of consequences. In stiff or hard material the CSD spends additional energy cutting more material than it excavates, leading to reduced efficiency and greater wear. In areas where the cut depth is restricted, spillage limits the borrow area yield or requires costly cleanup to leave grade.

In the water column, plumes resulting from spillage may cause environmental loss as light reduction and sedimentation affect sensitive receptors (Becker et al., 2014; Nakai, 1978). Also, turbidity plumes can reduce oxygen levels and interfere with fish respiration and feeding. Furthermore, the release of adsorbed pesticides, herbicides, toxic metals and synthetic organic compounds may contaminate the water column (Nakai, 1978). Simultaneously, environmental gains are to be expected from the release of nutrients and the supply of fine sediments to silt rich habitats (Becker et al., 2014).

Six types of spillage sources pertaining to CSD cutting are identified. A brief overview of the types of spillage is given below, followed by a detailed discussion of the first type, spillage due to high rotational velocity-induced advection (centrifugal advection). As of yet, in literature, no analytical models exist that describe spillage due to centrifugal advection. This paper presents a preliminary pseudo-analytical model for spillage due to centrifugal advection and calibrates the model using experimental data taken from Den Burger (2003). Since it is difficult to quantify individual spillage source, CSD spillage is the sum of individual spillage terms.

### Rotational Velocity-Induced Advection

High rotational velocity-induced spillage is a primary spillage source for CSD cutting. In its axial trajectory towards the suction mouth, entrained aggregates are accelerated by a centrifugal force induced by the rotational moment of the cutter, resulting in centrifugal advection along the cutter contour. Centrifugal advection leads to a plume in the water column before sediments redeposit into the bed. This type of spillage is most pronounced with small grain sizes, high rotation speeds and low mixture velocities. Figure 1 schematically depicts the trajectory of a single particle for the over- (a) and under-cut (b) scenario. Although not identical, centrifugal advection spillage of similar magnitude is observed for each flow pattern (den Burger, 2003). This type of spillage  $S_1$  [-] is investigated in this paper.

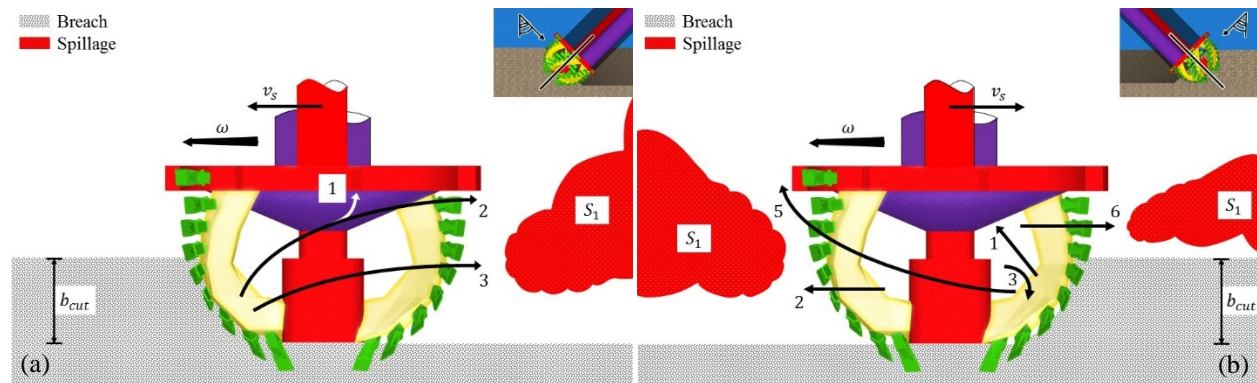


**Figure 1:** Centrifugal advection spillage for over-cutting (a) and under-cutting (b) as found in particle trajectory experiments by Den Burger. Particle trajectories relevant to high rotational velocities are denoted with numbers 1,2,3,5,6. A fourth trajectory was neglected at higher velocities.

### Rapid Redeposition

The suspension acceleration resulting from mechanical excavation of the blades may be offset by the influence of gravity. Therefore, solids that are suspended from the bank may rapidly redeposit. Spillage from rapid redeposition  $S_2$  [-] is highly dependent on particle size and rotational velocity. This can be explained by the higher inertia of larger particles that are more difficult to suspend. Industry observations indicate a significantly lower production rate for over-cutting scenarios. In over-cutting, the tangential velocity of the front and top blades coincide with the gravity vector and swing velocity respectively. Dislodged sediment will therefore accelerate downwards and through the suction zone of influence to redeposit immediately (see Figure 2a). In under-cutting, the opposing rotational and

gravitational force vectors result in a particle trajectory characterized by relatively high suspension rates and improved mixing in the cutter as depicted in Figure 2b. Sediment passes through the suction zone of influence with lower velocity.

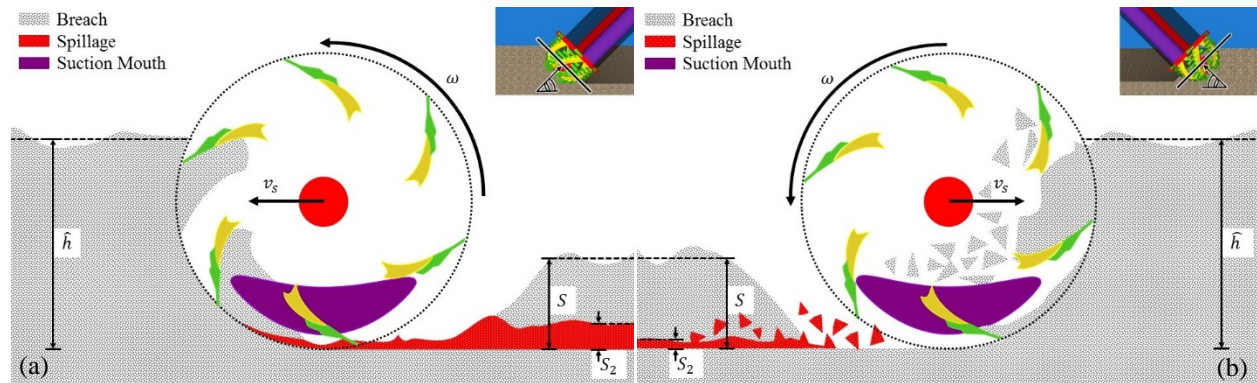


**Figure 2:** Rapid redeposition-induced spillage for over-cutting (a) and under-cutting (b).

### Violent Cutting

Violent cutting is a CSD aspect that pertains to particle suspension and subsequent transportation to an area beyond reach of the CSD head. As the blades and teeth (or chisels for sand cutting) of the cutter head penetrate the bank, soil disintegrates in front of the cutter and some particles will be lifted due to the rotational motion of the cutter head as depicted in Figure 3a. Moreover, a high swing velocity can cause a bull-dozing effect on the bank which lifts and suspends particles. Particles that redeposit in front of the cutter may be encountered by the cutter head again. Particles that settle behind the cutter contribute to spillage. This type of spillage is most visible when digging rock and cemented material.

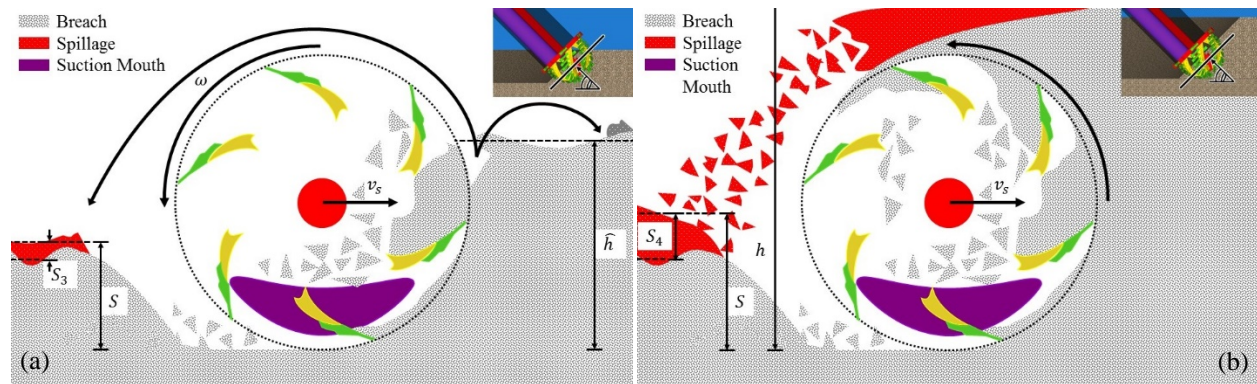


**Figure 3:** Spillage due to violent cutting (a) and spillage due to buried cutting (b) for an under-cutting scenario.

### Buried Cutting

When dredging a bank height that exceeds the effective height of the cutter head, the undermined soil will fail and rest onto the cutter head. Generally, this soil volume will be entrained into the cutter head, thereby increasing production. However, the cutter head might reach saturation, upon which remaining particles will move past the cutter head and fall behind the cutter head as illustrated in Figure 3b. Spillage due to buried cutting  $S_4$  [-] is generally determined by the height of the bank and the swing speed.

### Breaching

When the cutterhead breaches the bank, the slope angle of the breach may be larger than the internal friction angle of the bank material. With the absence of capillary forces below the water line, the steep slope will cause bank instability for granular materials. Van Rhee et al. (1998) describes that the bank wall following a dredger passage can be temporarily steep for sand due to dilatancy-induced plastic deformation of the breach. Shear deformation increases

the pore volume of sand and an increased dilatancy causes an under-pressure in the pores resulting in an inflow of water. This process temporarily increases the effective pressure on the bank, yielding a temporarily stable bank slope. The slope will collapse when maximum possible dilatancy is reached.

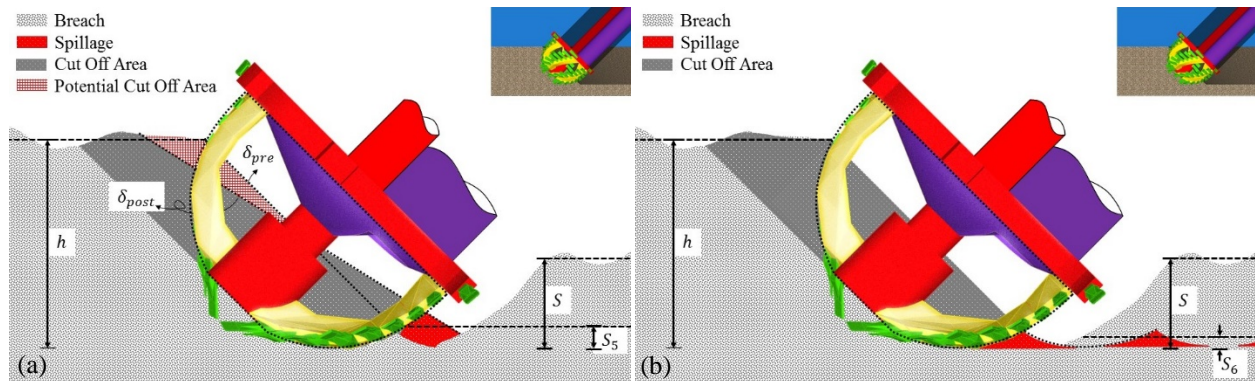


**Figure 4:** Spillage due to bank instability (a) and spillage due to cutter geometry (b).

Figure 4a depicts a situation in which the bank wall has collapsed after the cutter passes. It can be seen that the newly created slope extends towards the area that has already been dredged. Hence, this soil remains on the seabed and is considered spillage. Spillage due to bank instability  $S_5$  [-] is mostly dependent on the porosity, particle size and the swing speed.

#### ***Unstable Breaching***

When the slope angle below a temporary stable wall is smaller than the existing slope angle, the breaching process is considered unstable (van Rhee et al., 1998). According to Van Rhee (2018), unstable breaching may occur at stationary bulk dredging operations with large bank heights where spillage is less relevant.

#### **Cutter Geometry**

Inherent to the geometry of the cutter head, a relatively small spillage source  $S_6$  [-] can be observed. As the cutter travels forward in discrete step sizes, a portion of the soil above the lower cutter tip depth is undisturbed (see Figure 4a). Based on tradeoffs between the magnitude of inertia and the irregularity of cut areas, cutter geometry has evolved from cylindrically-shaped heads to parabolically-shaped heads (Vlasblom et al., 2006).

#### **Other Factors: Vessel Movement and Survey Disparity**

Operations in ports, canals, rivers and offshore locations makes the CSD subject to a variety of environmental conditions. Translational and rotational vessel movements such as surge, heave and pitch result in unexpected cutter head movements. Furthermore, soil type estimations and bathymetry measurements are complex and prone to errors. The effect of vessel movement and erroneous estimations are inherently difficult to measure directly, and can magnify other spillage sources.

### **EXISTING MODELS FOR SPILLAGE**

The three dimensional nature and complex geometry of the cutterhead, combined with the inability to accurately quantify spillage types encumber CSD spillage modeling and validation. Additionally, observations from experiments and empirical models are subject to scaling difficulties. The mechanical excavation of the cutter scales according to Froude's number since inertial and gravitational forces are governing. However, the suction mouth process is characterized by dominant inertial and viscous forces, rendering Reynolds scaling most appropriate. When gravity and viscosity dominate, the model becomes highly sensitive to the viscosity and density (Slotta, 1978).

#### **Empirical models**

Industry practices commonly estimate spillage by linearly scaling the total amount of fines subject to dislodgement by an empirically-derived coefficient as evidenced by equation (1) (Becker et al. 2014). This expression presumes that a certain fraction of fines is representative or in its entirety responsible for spillage due to centrifugal advection.

$$m_{eq} = \sigma_{eq} \rho_d V_{situ} f_{<63\mu m} \quad (1)$$

Where  $m_{eq}$  is the total cutter head related mass of fines (dry solids) brought into suspension [kg],  $\sigma_{eq}$  is an empirical source term fraction associated with cutter head spillage [-],  $\rho_d$  is the dry solids density [kg/m<sup>3</sup>],  $V_{situ}$  is the in situ dredge volume [m<sup>3</sup>] and  $f_{<63\mu m}$  is the fraction of fines smaller than 63  $\mu m$  [-]. The fraction of fines during the dredge operation may increase due to degradation (Ngan-Tillard et al, 2009). Empirical source term fractions are typically proprietary data.

### **Regression Analyses**

Joanknecht (1976) found empirical relations for dimensionless similitude criteria obtained from experimental data for a cylindrical cutterhead. It was observed that Froude scaling complemented with the ratio of the terminal velocity and the mixture velocity resulted in appropriate scaling. The experiments indicated that over-cutting spillage was positively correlated with the ratio of the swing velocity  $v_s$  and the tangential velocity, whereas under-cutting spillage remained insensitive to this ratio.

Slotta (1978) utilized the Buckingham  $\Pi$  theorem to find empirical relations with the Euler, Reynolds and Froude numbers as well as a diameter ratio and a ratio of the rotational velocity and the mixture velocity. Experimental data indicated that Reynolds scaling should be applied for the suction inlet.

Hayes (1986) performed a linear regression study for dimensionless variable groups obtained from observed suspended sediment concentrations resulting from CSD operations at Calumet harbour (Hayes et al. 1988). Collins (1995) expanded this dataset with three field operations and two experimental studies and performed a similar linear regression. The improved empirical model could, however, “not explain suspended sediment variations very well” (Hayes et al., 2000). Earlier research by Andrassy et al. (1988) in which CSD operation parameters were used in a correlation study for a similar dataset, was unable to identify statistically significant relationships.

Hayes et al. (2000) performed a dimensional criteria study to support a dimensionless regression analysis based on Buckingham  $\Pi$  theorem to find spillage correlations. The “106 observation data set used in this study represents a too limited range of operating parameters to generate model applicable to a wider variety of conditions”, however reasonable accuracy was obtained for spillage data. Additional validation is needed to substantiate the model.

### **Numerical models**

A joint research effort from a group of Dutch contractors united under the name Combinatie Spuurwerk Baggertechniek (CSB), Ministerial Agency of Public Works Rijkswaterstaat and research institute WL|Delft Hydraulics conducted a series of experiments to gain a better understanding of the internal flows in and around the cutter. As summarized by Den Burger (2003), the experiment results indicate that the cutter head resembles a combination of an axial pump as well as a centrifugal pump.

The mixture velocity was varied in the experiments at WL|Delft Hydraulics. Depending on the mixture velocity, a transition value was observed for the rotational velocity. The data showed that there is an inward flow along the entire contour of the cutter head for rotational velocities below the transition value. However, above this threshold an outwards flow near the back plate was observed that increased with rotational velocity. This outward flow contains suspended particles which may not re-enter the cutter head. Figure 5 schematically depicts the flow that is generated by these pump effects as well as the location along the contour line of the cutter head where inflow reverses to outflow.

Interestingly, particle trajectories in the under-cut and over-cut situation were very different. However, for both situations they appeared insensitive to variations of the rotational velocity and mixture velocity. Also, the ratio of the transition value for the rotational velocity and the mixture velocity appeared relatively constant and identical for the under-cut and over-cut situation. Den Burger describes that the rotational velocity and mixture velocity do influence the magnitude of the velocities in both situations as was found by Moret (1977a).

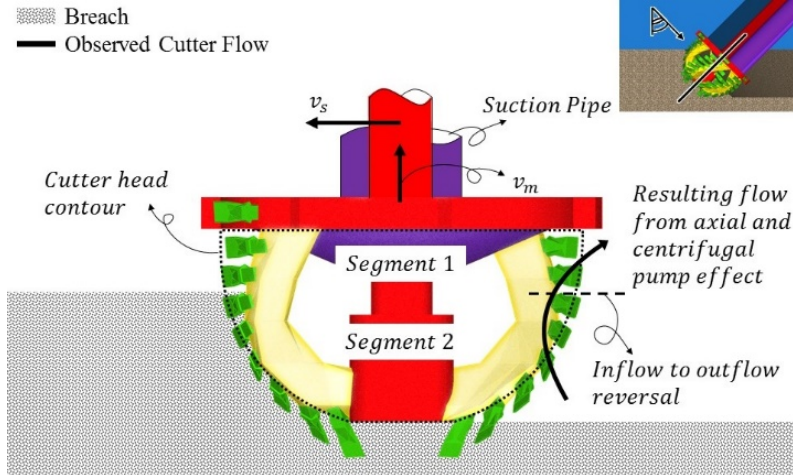


**Figure 5:** Schematic representation of the flow resulting from the axial and centrifugal pump effect.

### MODEL DEVELOPMENT

Miedema (2017) and Nieuwboer (2017) conceptualized a pseudo-analytical model based on Den Burger's observations. In this paper, a heavily simplified preliminary model is presented in which only spillage due to centrifugal advection is considered ( $S_1$ ). A virtual radial discharge impeller is hypothesized in the cutterhead. The impellers simulate the influence of the rotation of the cutter head on the hydraulic transport inside the cutterhead. It is assumed that the cutterhead contains infinitely many virtual impeller blades with infinitesimally small blade thicknesses. The impellers are presumed geometrically similar and operated at dynamically similar conditions.

#### Similarity of Flow

Let us consider flow similitude for a centrifugal pump, i.e. the ratio of the average fluid velocity  $c$  [m/s] and the tangential impeller velocity  $u$  [m/s] equals a constant dimensionless flow number

$$\frac{c}{u} = \Phi \quad (2)$$

Where  $\Phi$  represents the flow number [-]. The average fluid velocity exits the pump over an area equal to the circumference of the pump, multiplied by the impeller width and limited by a factor  $\Gamma$  [-] that accounts for limitations to the outflow area, i.e.  $\Gamma\pi Db$ . Assuming incompressible flow and flow equilibrium, the fluid velocity inside the volute chamber follows from volume continuity and reads

$$c = \frac{Q}{\Gamma\pi Db} \quad (3)$$

Where  $Q$  is the pump discharge [ $\text{m}^3/\text{s}$ ],  $D$  is the pump diameter [m] and  $b$  the impeller width [m]. The tangential velocity of the impeller is found through multiplication of the angular velocity  $\omega$  [rad/s] and the cutter radius [m] ( $u = \omega D/2$ ). Substitution of the velocity ratio in equation (2) and subsequent reordering yields an expression for the discharge as a function of the angular velocity as evidenced in equation (4).

$$Q = \Phi \frac{\pi}{4} \Gamma b \omega D^2 = \hat{\Phi} \Gamma b \omega D^2 \quad (4)$$

Where  $\hat{\Phi}$  is an adapted flow number [-]. Physically, the coefficient  $\hat{\Phi}$  can be considered a dimensionless ratio of the velocity components in the tangential direction and the radial direction. The fluid viscosity is captured by this dimensionless measure.

**Centrifugal Pump Pressure**

Simulating a pump effect for the cutter head requires an expression for the force that is exerted by the fluid on the hypothetical volute chamber. This centrifugal force for a rotating mass is given in equation (5).

$$F_{cf} = \frac{2\Psi mu^2}{D} \tag{5}$$

Where  $m$  is the fluid mass ( $\rho\pi/4D^2b$ ) inside the cutter [kg] and  $\Psi$  is a coefficient that scales the centroid of the fluid mass [-]. The meridional exit area  $A$  [m<sup>2</sup>] of the virtual volute chamber equals  $\pi Db$ , hence the internal pressure  $p^-$  [Pa] that is exerted on the volute chamber can be found by again substituting  $u = \omega D/2$

$$p^- = \frac{1}{8}\Psi\rho\omega^2D^2 = \hat{\Psi}\rho\omega^2D^2 \tag{6}$$

Expressions (4) and (6) can be combined in order to find the volumetric flow rate induced by the angular velocity of the supposed centrifugal effect, and rewritten, to find the induced pressure as a function of the angular velocity.

$$Q = \frac{\hat{\Phi}\Gamma p^- b}{\hat{\Psi} \rho\omega} \Leftrightarrow p^- = \frac{\hat{\Psi} \rho\omega Q}{\hat{\Phi}\Gamma b} \tag{7}$$

**Distinguishing Flow Terms**

For this preliminary model, a series of assumptions is made. First, water is taken incompressible and fluid densities are considered equal for all flow terms. Second, hydraulic transport through the bank is neglected. Third, the open cutterhead is considered a control volume and is divided into segment 1 and 2, with the latter closest to the bank. The interface between these segments is located at the cutter diameter where inflow reverses to outflow (see Figure 5). An outflow  $Q_1$  at segment 1 may (partially) return inside the control volume at segment 2, where an inflow  $Q_2$  is considered.

The volumetric flow rate for the dislodged bank material into the cutter is  $Q_c$  and an independent volumetric flow rate  $Q_p$  represents the flow withdrawn by the suction mouth. Inflows into the control volume will have a positive contribution and outflows have a negative contribution. The volume balance equation for the control volume reads

$$Q_c - Q_p - Q_1 + Q_2 = 0 \tag{8}$$

Where  $Q_i$  denotes the volumetric flow rate [m<sup>3</sup>/s]. Figure 6 schematically represents the flow pattern as found by Den Burger (2003) with the given volumetric flow rates as viewed from above (a) and in front (b).

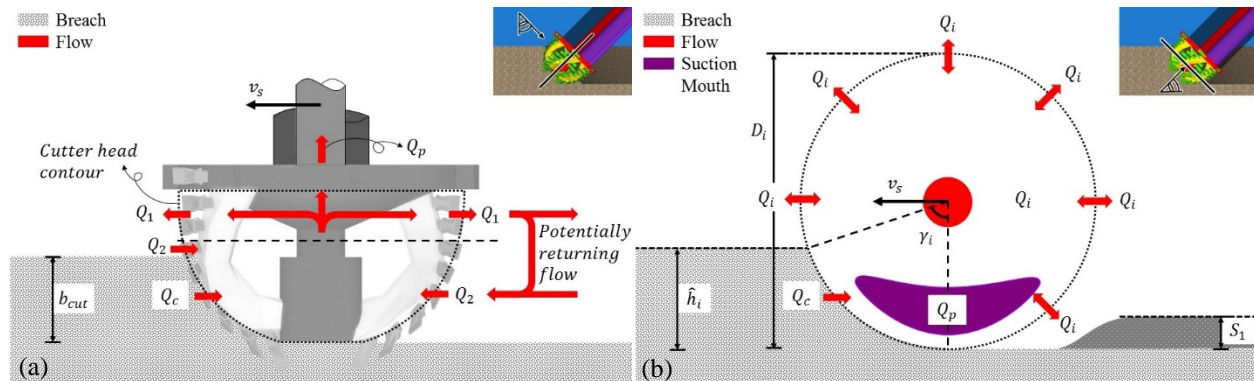


**Figure 6:** Simplified representation of flow pattern in and around the cutter from a top perspective (a) and front perspective (b).

Early results indicate it is safe to assume that there is net outflow in segment 1 provided that the rotational cutterhead velocities in the working range of CSD operations (~30 [rpm]). Hence the positive and negative flow terms per

segment implicitly describe the axial pump effect inside the control volume since there must be hydraulic transport from segment 2 to segment 1.

### Cutter Geometry

In order to describe the flows in this model, the control volume is heavily simplified by reducing the cutter head geometry to a segmented cylinder geometry. First, the geometry is reduced to a truncated cone shape. Next, the cylinder diameters are found through linear interpolation within the truncated cone. These diameters are representative for the flow through the full heights  $b_1$  [m] and  $b_2$  [m] of the respective segments of the cutter as depicted in Figure 7a and expressed in equations (9) and (10).

$$D_1 = D_{ring} - \frac{b_1}{2 \tan \kappa} \quad (9)$$

$$D_2 = D_{top} - \frac{b - b_1}{2 \tan \kappa} \quad (10)$$

Where  $D_1$  is the average diameter of segment 1 [m],  $D_2$  is the average diameter of segment 2 [m],  $D_{ring}$  is the diameter of the cutter ring [m],  $D_{top}$  is the diameter of the cutter top [m] and  $\kappa$  represents the angle between the truncated cone and the cutter ring [deg].

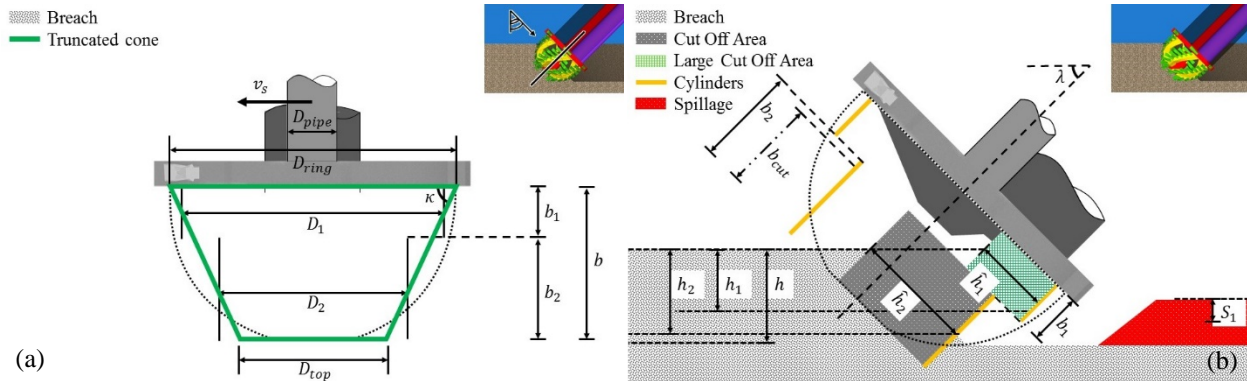


**Figure 7:** Simplification of the cutter geometry (a) and schematic visualization of the relation between bank height and effective bank height (b).

### Bank Geometry

For simplicity purposes, the cutterhead is considered penetrated in the bank under an angle  $\lambda$  [deg] into an equally inclined bank angle of 45 degrees. In reality, this is highly uncommon since the high suction mouth placement induces rapid redeposition. Figure 7b depicts the cutter placement for this model. The cut off area of the bank  $A_{cut}$  [m<sup>2</sup>] is related to the placement of the cutter and can be mapped onto the segmented cutterhead shape by introducing the effective bank height  $\hat{h}$  [m], i.e. the height of the bank in the coordinate system of the cutter. Choosing a lower bank height  $h$  [m] and thus effective bank height allows for the distribution of cut face towards segment 2 of the simplified shape. It is assumed that the tip of the simplified cutter geometry can be identified as the lower end of the effective bank height of segment 2  $\hat{h}_2$  [m].

As depicted in Figure 6b, the angle  $\gamma_i$  [rad] associated with the intersecting circumference of the cutter and the bank geometry can be expressed as a function of the cutter diameter and effective bank height as evidenced in equation (11). Note that this equation is only valid when the bank and ladder angle are equal and for  $\hat{h}_i \leq 2D_i$ . Additional geometry formulations are necessary for larger bank heights.

$$\hat{h}_i = \frac{D_i}{2}(1 - \cos \gamma_i) \Leftrightarrow \gamma_i = \cos^{-1} \left( 1 - \frac{2\hat{h}_i}{D_i} \right) \quad (11)$$

Discretization of the cutterhead requires a geometry criterion to determine segment contributions to the cut face. Equation (12) relates a linearized cut depth to the cut off area.

$$b_{cut} = \frac{A_{cut}}{\hat{h}} \quad (12)$$

Where  $b_{cut}$  is an estimate for the depth of the cut for the given bank-cutter interaction. Consequently, a sequence of geometry expressions allow for the computation of the parameters relevant to the cutting contributions of segment 1 and 2 for any given  $D_1$  and  $D_2$  as outlined in equation (13) and (14).

$$\hat{h}_2 = \begin{cases} \frac{A_{cut}}{b_2}, & b_{cut} < b_2 \\ \hat{h}, & b_{cut} \geq b_2 \end{cases} \quad (13)$$

$$\hat{h}_1 = \begin{cases} 0, & b_{cut} < b_2 \\ \frac{A_{cut} - \hat{h}_2 b_2}{b_1}, & b_{cut} \geq b_2 \end{cases} \quad (14)$$

Where  $\hat{h}_1$  is de effective bank height of segment 1 [m]. Since flows through soil are neglected, the active flow contribution areas of segment 1 and 2 are found using the bank contact angle  $\gamma_i$  [rad] (see Figure 6b). The bank contact angle is used to determine the dimensionless factor  $\Gamma_i$  [-] that was introduced to account for the free flow factor of the impeller exit area as shown below

$$\Gamma_i = 1 - \frac{\gamma_i}{2\pi} \quad (15)$$

### Fundamental Pressure Assumption

The pressures  $p_1^-$  and  $p_2^-$  generated by the virtual impeller on exerted on the virtual volute chambers of segment 1 and segment 2 [Pa] can be found using equation (7). The adapted dimensionless coefficients are considered equal for both segments by assuming dynamic similarity of flow, i.e. Reynolds number scaling. Note that these pressures  $p_1^-$  and  $p_2^-$  as given below are denoted as negative due to their corresponding velocity directing outwards of the control volume.

$$p_1^- = \frac{\hat{\Psi}}{\hat{\Phi}\Gamma_1} \frac{\rho\omega Q_1}{b_1} \quad (16)$$

$$p_2^- = \frac{\hat{\Psi}}{\hat{\Phi}\Gamma_2} \frac{\rho\omega Q_2}{b_2} \quad (17)$$

In a realistic two-dimensional situation, as depicted in Figure 8a, the pressure  $p_1^-$  (red) and  $p_2^-$  (green) along the segmented control volume are expected to drop quadratically upon further propagation into the surrounding environment of the cutter. In this pseudo-analytical model, the interaction of the pressures outside the control volume is heavily simplified as depicted in Figure 8b.

Miedema (2017) proposes a fundamental pressure assumption for the contour of segment 2 by relating the potentially returning flow of from segment 1 to the pressure outside of segment 2. It is assumed that the pressure that is generated by the centrifugal pump in segment 1 remains constant over a wide area beyond the control volume, including at the boundary of segment 2. Moreover, the external propagation of the pressure that is generated internally at segment 2 is neglected outside of the control volume. Consequently, the pressure at the contour of segment 2 reads

$$p_2^+ = p_2^+ = p_1^- \quad (18)$$

Justification of the fundamental assumption of an equal pressure contour centered around the boundary of segment 1 is subject to discussion. It can be argued that the square relation between the pressure and the segment diameter allows for a significantly larger pressure generation at segment 1, rendering the generated pressure at section 2 negligible.

Secondly, in reality the dimensionless coefficient  $\hat{\Psi}_i$  from equations (16) and (17) will be higher for segment 2 due to the fact that larger impellers are more efficient. This supports the assumption that  $p_1^-$  is significantly larger than  $p_2^-$ .

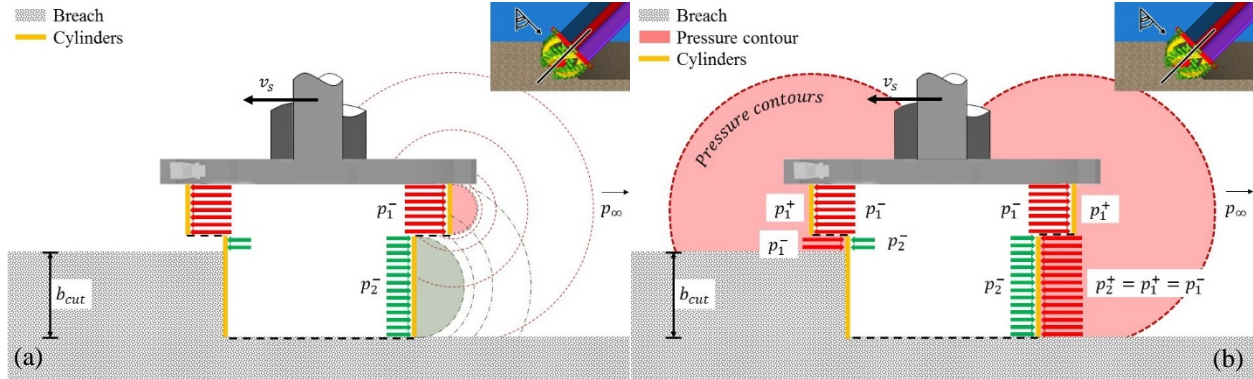


**Figure 8:** Expected external pressure contours (a) and pressure contours according to Miedema (b).

In contrast, upon the addition of different densities in the pressure generating segments, the density of the inflow  $Q_2$  would be smaller than that of  $Q_1$  due to the fact that the suspended sediment is larger inside the control volume and particles may not re-enter the cutterhead. Since  $p_1^+$  will be generated with a higher density, the lower density of the inflow at section reduces affects the assumed propagation of pressure from segment 1. Additionally, the pressure at segment 1 acts on the full circumference of the segment, whereas equation (15) indicates that the acting pressure at segment 2 is limited by a relatively larger bank contact area ( $\Gamma_2 > \Gamma_1$ ). In conclusion, the assumption should be substantiated with further research but can be used for a preliminary model.

#### Derivation of Volumetric Flow Rates

The volumetric flow rate at segment 1 can be found using the discharge-pressure relationships of equation (7), repeated here for clarity

$$Q_i = \frac{\hat{\Phi}\Gamma_i p_i b_i}{\hat{\Psi} \rho_i \omega} \quad (19)$$

Since this model assumes outflow at segment 1, the vicinity of segment 1 to the suction mouth requires a flow condition that guarantees positive or zero flow despite the suction pressure generated by the suction inlet.

$$Q_1 = \begin{cases} \frac{\hat{\Phi}\Gamma_1 p_1^- b_1}{\hat{\Psi} \rho \omega}, & Q_1 \geq 0 \\ 0, & Q_1 < 0 \end{cases} \quad (20)$$

#### Flow circulation

The volumetric flow rate from equation (20) can be adapted to find an expression for the specific flow rate  $q_i$  per unit width of the cutter [ $\text{m}^2/\text{s}$ ]. Implicitly, a function for the difference in specific flow rate can be found as a function of the pressure gradient as specified in the latter expression of equation (21).

$$q_i = \frac{\hat{\Phi}\Gamma_i p_i}{\hat{\Psi} \rho \omega} \Rightarrow \Delta q_i = \frac{\hat{\Phi}\Gamma_i \Delta p_i}{\hat{\Psi} \rho \omega} \quad (21)$$

With  $p_2^+ = p_1^+ = p_1^-$  from equation (18), the resulting pressure gradient over the boundary of segment 2 reads

$$\Delta p_2 = p_2^+ - p_2^- = p_1^- - p_2^- \quad (22)$$

Substitution of equation (22) in equation (21) results in an expression for  $Q_2$  as evidenced in equation (23).

$$Q_2 = \Delta q_2 b_2 = \frac{\hat{\Phi}\Gamma_2 \Delta p_2}{\hat{\Psi}} \frac{b_2}{\rho\omega} = (p_1^- - p_2^-) \frac{\hat{\Phi}\Gamma_2}{\hat{\Psi}} \frac{b_2}{\rho\omega} \quad (23)$$

### In Situ Dredge Flow Rate

The in- and outflow of water at the cutterhead due to the swing velocity  $v_s$  [m/s] is considered negligible. Finding an expression for the volumetric flow rate of the suspended sediment  $Q_c$  involves determining the flow of sediment that enters the control volume as the cut off area  $A_{cut}$  moves through the bank with swing velocity  $v_s$  [m/s]. The in situ dredge flow rate is approximated by

$$Q_c = A_{cut} v_s \quad (24)$$

### Production Flow Rate

The volumetric flow rate of the production flow  $Q_p$  is subject to variations of the suction inlet velocity and is easily found as

$$Q_p = \pi R_{pipe}^2 v_m \quad (25)$$

Where  $R_{pipe}$  is the radius of the suction pipe [m] and  $v_m$  the mixture velocity through the suction mouth [m/s]. Figure 9 provides an overview of the volumetric flow rates.

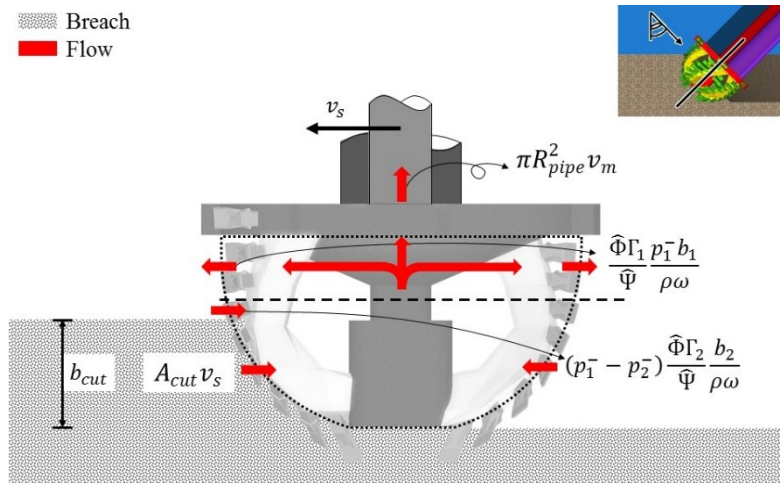


Figure 9: Final expressions for volumetric flow rates in the cutter control volume.

### Derivation of Segment Widths

Substitution of equation (20) and (23) in equation (8) results in an equation for the volumetric flow rate given as

$$Q_c - Q_p - \frac{\hat{\Phi}\Gamma_1 p_1^- b_1}{\hat{\Psi}} \frac{b_1}{\rho\omega} + (p_1^- - p_2^-) \frac{\hat{\Phi}\Gamma_2}{\hat{\Psi}} \frac{b_2}{\rho\omega} = 0 \quad (26)$$

Multiplication of equation (26) by  $(\hat{\Psi}/\hat{\Phi})(\omega/p_1^-)$  yields

$$\frac{\hat{\Psi}}{\hat{\Phi}} \frac{\omega}{p_1^-} (Q_c - Q_p) - \Gamma_1 \frac{b_1}{\rho} + \Gamma_2 \frac{(p_1^- - p_2^-) b_2}{p_1^- \rho} = 0 \quad (27)$$

Subsequent substitution of  $b_2 = b - b_1$  as well as  $p_1^- = \hat{\Psi}\rho\omega^2 D_i^2$  from equation (6) gives

$$\frac{1}{\hat{\Phi}} \frac{1}{\rho\omega D_i^2} (Q_c - Q_p) - \Gamma_1 \frac{b_1}{\rho} + \Gamma_2 f \frac{b - b_1}{\rho} = 0 \quad (28)$$

Where  $f = (D_1^2 - D_2^2)/D_1^2$  [-]. The objective is to find the location on the contour line where the flow reverses from inflow to outflow, i.e. the magnitudes of or ratio between of  $b_1$  and  $b_2$ . Hence,  $b_1$  is isolated on the left hand side to obtain

$$b_1 = \frac{\Gamma_2 f b + \frac{1}{\hat{\Phi}} \frac{1}{\omega D_i^2} (Q_c - Q_p)}{(\Gamma_1 - f \frac{\Gamma_2}{\Gamma_1})} \quad (29)$$

Equation (29) is multiplied by  $(\hat{\Phi} \Gamma_1 \omega D_1^2) / (\hat{\Phi} \Gamma_1 \omega D_1^2)$  and rearranged to obtain a more elegant expression for  $b_1$

$$b_1 = \frac{\hat{\Phi} \Gamma_2 (D_1^2 - D_2^2) b \omega + Q_c - Q_p}{\hat{\Phi} (\Gamma_1 - \Gamma_2) D_1^2 \omega + \hat{\Phi} \Gamma_2 D_2^2 \omega} \quad (30)$$

Finally, equation (30) is substituted with  $Q_c$  and  $Q_p$  as found in equation (24) and (25) respectively to yield an expression for  $b_1$  that is based on geometric and dimensional operational parameters as well as the dimensionless number  $\hat{\Phi}$ . Since the segment height cannot be rendered negative due to the volumetric flow rate  $Q_1$ , a requirement is set so that  $b_1 > 0$ . The expression for the height of segment 1 reads

$$b_1 = \begin{cases} \frac{\hat{\Phi} \Gamma_2 (D_1^2 - D_2^2) b \omega + A_{cut} v_s - \pi R_{pipe}^2 v_m}{\hat{\Phi} (\Gamma_1 - \Gamma_2) D_1^2 \omega + \hat{\Phi} \Gamma_2 D_2^2 \omega}, & b_1 \geq 0 \\ 0, & b_1 < 0 \end{cases} \quad (31)$$

### Iterative Solution

The diameters from Equation (31) use expressions for the cutter diameters as described in equation (9) and (10). This is an implicit problem due to the interdependency of the diameters  $D_1$  and  $D_2$  and heights  $b_1$  and  $b_2$  respectively. Consequently, this implicit problem should be solved through iteration of  $b_1$  using a threshold value for accuracy. A solution approach is given in Figure 10.

```

1 Find A from data
3 Determine h
4 Compute  $\hat{h} = h \sin(90 - \lambda)$ 
5 Compute  $b_{cut}$  Eq. (12)
6 Set convergence coefficient relax
7 Set accuracy coefficient threshold
8 Estimate  $\widehat{b}_1$ 
9 While error > threshold
10    $\widehat{b}_2 = b - \widehat{b}_1$ 
11   Compute  $D_1$  and  $D_2$  Eq. (9) and (10)
12   Compute  $\widehat{h}_2$  and  $\widehat{h}_2$  Eq. (13) and (14)
13   Compute  $\gamma_1$  and  $\gamma_2$  Eq. (11)
14   Compute  $\Gamma_1$  and  $\Gamma_2$  Eq. (15)
15   Compute  $b_1$  Eq. (31)
16   error =  $|b_1 - \widehat{b}_1|$ 
17    $\widehat{b}_1 = \widehat{b}_1(1 - \textit{relax}) + b_1(\textit{relax})$ 
18 End
```

**Figure 10:** Example script for computation of  $b_1$  with references to equation numbers in parentheses.

### Adding Suspended Sediment

The purpose of this simplified model is to find an expression for spillage. It was assumed that the densities of the flow terms are equal. To obtain a representation of spilled sediment, the flow terms are retrospectively complemented with a concentration measure  $c_i$  for the amount of suspended solids per unit volume [-]. Caution with the model results should be observed since the actual effect of suspended solids on flow density is neglected in this preliminary model.

It is assumed that hydraulic transport is homogeneous in concentration within segment 1, i.e.  $c_p = c_1$  with  $c_1$  being the concentration of the hydraulic transport exiting the cutter head at segment 1 [-] and  $c_p$  being the concentration of the production flow that is sucked up to the vessel [-]. A concentration  $c_c$  of the volumetric flow rate of the cut flow is considered [-] as well as a concentration  $c_2$  for the volumetric flow rate  $Q_2$  [-] that is assumed zero. This assumption neglects the effect of suspended particles recirculating from segment 2 to segment 1. Figure 11 depicts an overview of the flows.

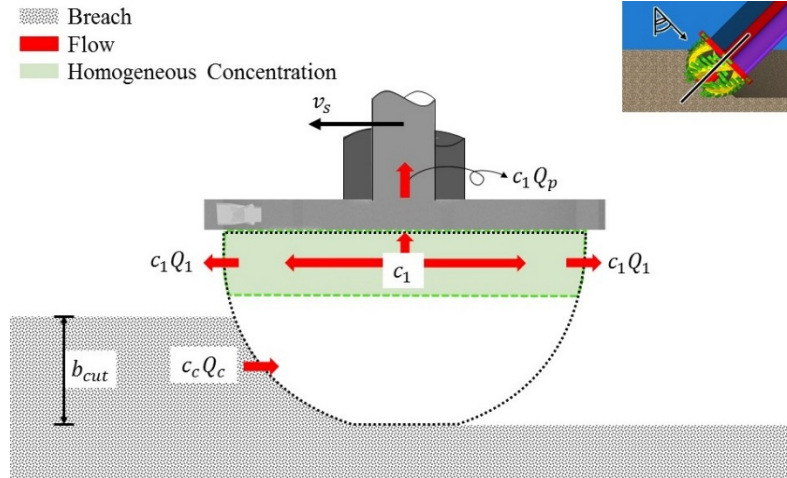


**Figure 11:** Schematic depiction of assumed concentrations inside the control volume.

The considered mass flow rate balance reduces to equation (32) from which the concentration  $c_1$  directly follows. The outflow concentration should not exceed the inflow concentration, hence a condition is added in equation (33) to maintain sensible results.

$$Q_c c_c - c_1 Q_p - c_1 Q_1 = 0 \quad (32)$$

$$c_1 = \begin{cases} \frac{Q_c c_c}{Q_1 + Q_m}, & c_1 < c_c \\ c_c, & c_1 \geq c_c \end{cases} \quad (33)$$

Spillage due to centrifugal advection  $S_1$  can be found by computing

$$S_1 = \frac{c_1 Q_1}{c_c Q_c} \quad (34)$$

Which concludes a parameterized pseudo-analytical model for the determination of angular velocity-induced spillage.

### MODEL CALIBRATION

Supported by experiments, Den Burger (2003) found that particle trajectories in a CSD are governed by the centrifugal force  $F_{cf}$  in the cutter [N], the gravitational force  $F_g$  [N] and the product of the particle volume and radial pressure gradient in the suction mouth  $F_s$  [N]. The ratio of these terms provide a convenient alternative to known dimensionless scaling coefficients. Since this model focuses on centrifugal advection rather than rapid redeposition, the dominant spillage number is the ratio of centrifugal force and volume-pressure gradient product, i.e.

$$\frac{F_{cf}}{F_s} \propto \frac{\rho_p}{\rho_w} \left( \frac{\omega R_{ring}^3}{v_p R_{pipe}^2} \right)^2 \quad (35)$$

Where  $\rho_p$  is the particle density [kg/m<sup>3</sup>],  $\rho_w$  is the water density [kg/m<sup>3</sup>],  $R_{ring}$  and  $R_{pipe}$  are the cutter ring and pipe radii [m] and  $v_m$  is the mixture velocity [m/s].

### Flow Number

Calibration is chosen to be performed using an adapted dimensionless flow number  $\hat{\theta}$  [-] as derived from equation (35), which is the inverse of the flow number proposed by Steinbusch et al. (1999) and Dekker et al. (2003). This flow number was specifically deterministic for sand cutting as evidenced in analyses of experimental data from Mol (1977a) and Miltenburg (1983). The adapted flow number is defined as

$$\hat{\theta} = \frac{\omega R_1^3}{Q_p} \quad (36)$$

For calibration of the model, a dataset by Den Burger is used that contains production rates corresponding to adapted flow numbers for sand and rock. Data for rock were scaled obtained through experiments with gravel and scaled. An overview of experiment parameters is given in Table 1.

**Table 1** Experiment parameters for Miltenburg and Den Burger. <sup>1</sup> Sand diameter is presumed “similar to practice”. <sup>2</sup> Estimation for segmented values of the model. <sup>3</sup> Estimated value. <sup>4</sup> Only rock density given.

Property	Symbol	Sand (Miltenburg, 1983)		Rock (Den Burger, 2003)		Units
		Prototype	Experiment	Prototype	Experiment	
Particle diameter	$d_{50}$	180E-3 <sup>1</sup>	180E-3	80	10	mm
Bed concentration	$c_c$	0.4	0.4	0.42	0.42	-
Particle density	$\rho_p$	2650	2650	2200 <sup>4</sup>	2650	Kg/m <sup>3</sup>
Bulk density (wet)	$\rho_{b,wet}$	2000	2000	2200 <sup>4</sup>	2058	Kg/m <sup>3</sup>
Diameter of the cutter ring	$D_{ring}$	2.80	0.40	3.12	0.4	m
Diameter of the cutter top	$D_{top}$	2.11 <sup>2</sup>	0.18	2.11 <sup>2</sup>	0.28	m
Diameter of the suction pipe	$D_{pipe}$	0.7	0.1	0.95	0.1	m
Height of the cutter head	$b$	2.5 <sup>2</sup>	0.265	2.50 <sup>2</sup>	0.265	m
Swing velocity	$v_s$	0.2	0.1	0.2	0.1	m/s
Cut off area	$A$	1.4 <sup>3</sup>	0.023 <sup>2</sup>	1.4 <sup>3</sup>	0.03	m <sup>2</sup>
Bank angle	$\gamma$	$\pi/2$	$\pi/2$	$\pi/2$	$\pi/2$	rad
Cutter inclination angle	$\lambda$	45	45	45	45	deg
Rotational velocity	$\omega$	$\pi$	10/3 $\pi$	$\pi$	3 $\pi$	rad/s
Cutting scenario	-	under-cut	under-cut	under-cut	under-cut	-

It should be noted that the cutter inclination angle is non-typical for dredge operations since that would place the bottom of the suction mouth high relative to the bank. Conveniently, this parameter choice does benefit the calibration since spillage due to centrifugal advection is likely the governing spillage source. However, calibration is hindered since alternative spillage sources are expected as well.

Den Burger (2003) used the adapted flow number to perform a polynomial regression (n=2) to obtain the general trend for the production  $\eta$  [%] with respect to the velocity ratio  $\hat{\theta}$  for an under-cut scenario. Experiments suggested that for over-cutting “the trend of the production curve has changed” and requires further research. The preliminary model does not differentiate with respect to under- and over-cutting, but is calibrated on the under-cut experiments from Den Burger. Calibration is performed by finding a value for  $\hat{\Phi}$  for which spillage as a function of the velocity ratio follows the spillage curves from Miltenburg and Den Burger as found through  $S = 1 - \eta$ .

## Results for Sand

Figure 12 displays the model results for a comparison to sand data from Miltenburg. In graph (a), the experimental data and model results (spillage percentage) of three values for  $\hat{\Phi}$  are plotted against the flow number  $\hat{\theta}$ . Figure 12b displays the error for the plotted models [pp] as a function of the mixture velocity. The mixture velocity is found using a typical estimate of 30 revolutions per minute for large cutterheads. In this paper, Phi refers to the dimensionless ratio of the velocity components in the tangential direction and the radial direction and approximates the centrifugal pump effect.

For  $\hat{\Phi} = 0.22$ , the model curve as well as the standard deviation and double standard deviation of the difference with the experimental data is plotted. The other plots represent estimates for a lower ( $\hat{\Phi} = 0.20$ ) and upper ( $\hat{\Phi} = 0.23$ ) bound. The best approximation for Phi is visually identified with the objective for the mixture velocities to be accurate within a typical mixture velocity range of  $\langle 4,6 \rangle$  [m/s] as given by Miltenburg. For  $\hat{\Phi} = 0.22$ , the error falls within the 5 [pp] bandwidth for the applicable interval. Furthermore, the shape of the model plot appears to resemble that of the experimental results accurately, i.e. the model behaves according to expectations.

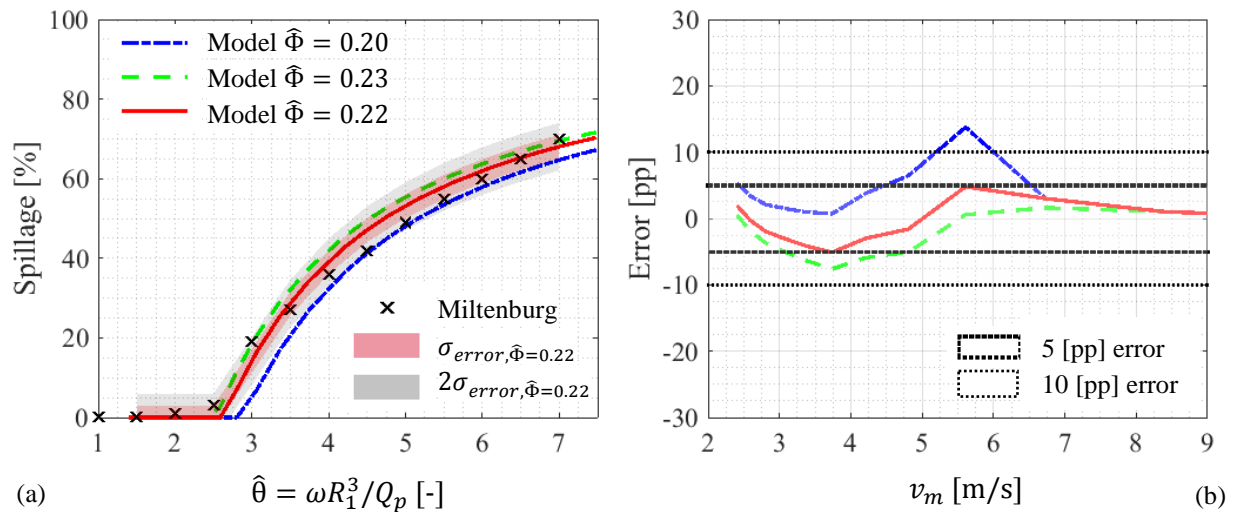


**Figure 12:** Spillage percentage vs. flow number  $\hat{\theta}$  (a) and error [percentage point] vs. mixture velocity (b) for sand.

## Results for Rock

The same estimation method and visualization method was used to find the model parameter  $\hat{\Phi}$  that corresponds best with experimental data from Den Burger that are scaled to represent the cutting of rock. Figure 13 displays the model curves (a) and errors (b) with respect to the experimental data. For  $\hat{\Phi} = 0.34$ , Reasonable model accuracy can be observed for flow numbers  $\hat{\theta}$  in the  $\langle 2,3 \rangle$  range corresponding to mixture velocities of approximately  $\langle 5,8 \rangle$  [m/s]. The typical CSD mixture range is best represented by the model with  $\hat{\Phi} = 0.41$  since the errors fall within the 10 percentage point bandwidth. However, the model curve does not follow the experimental data well.

For higher numbers of the velocity ratio, it can be observed that the spillage ratio is consequently underestimated for rock. This can be explained in a variety of ways. Firstly, the model is calibrated using data for scaled gravel that may include other spillage sources such as rapid redeposition. Secondly, the deviation suggests that the model is not capable of capturing the full centrifugal effect on larger suspended particles. Equation (35) can be used to demonstrate that an underestimation of the centrifugal force relative to the radial pressure gradient results in a quadratically smaller ratio of withdrawn particles whereas the flow number from equation (36) only scales linearly. Lastly, it is stressed that further research is required to verify the series of assumptions in the model and how larger particles are particularly affected.

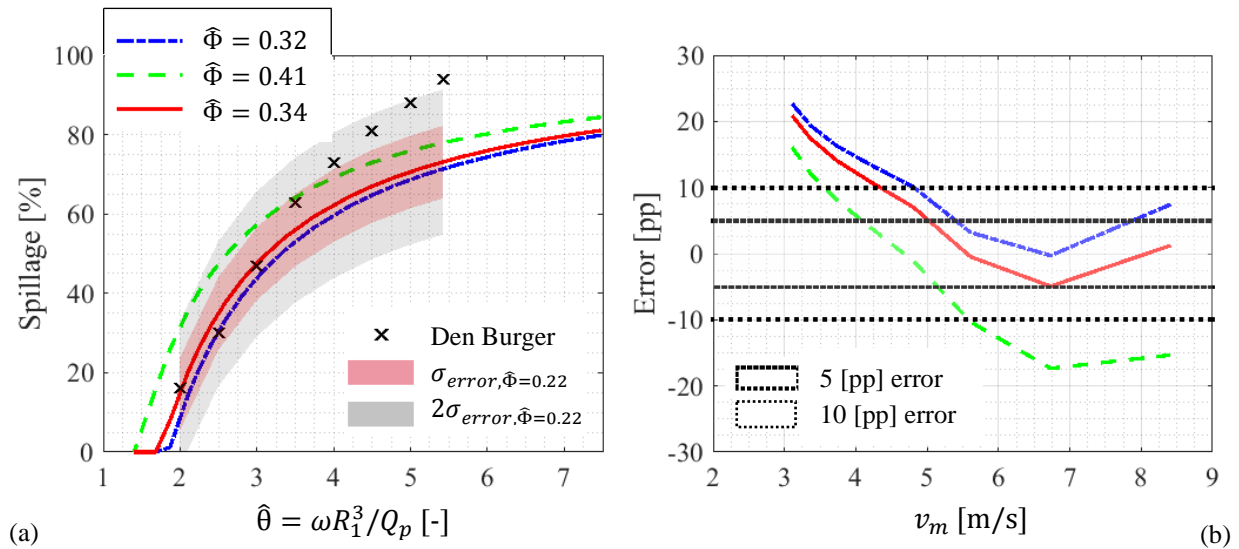


**Figure 13:** Spillage percentage vs. flow number  $\hat{\theta}$  (a) and error [percentage point] vs. mixture velocity (b) for rock.

## CONCLUSION

An adaptation of a dimensionless velocity ratio proposed by Steinbusch et al. (1999) and Dekker et al. (2003) is used as a governing number for model calibration using experimental data for sand from Miltenburg (1983) and rock from Den Burger (2003). Model parameters were identified for which sand spillage can be estimated within a 5 percentage point bandwidth of the experimental data. Moreover, the shape of the model plot appears to resemble that of the data for sand accurately, i.e. the model behaves as expected. The model underestimates spillage rates for rock-sized particles except at relatively low cutter speeds or high mixture flow rates, suggesting that either centrifugal advection is not the main source of spillage or that the model does not capture the centrifugal pump effect well for large particle diameters.

The most fundamental assumption in the model is the concept that the pressure outside the cutter is uniform and equal to the pressure generated near the cutter ring in segment 1. Furthermore, the model assumes a volumetric flow rate balance with equal densities for the terms. Currently, only two cutterhead segments are considered. Improvement of the model can be achieved by incorporating flow density differences and further discretization of the cutterhead. In combination with a further specification of the pressure gradient along the cutter contour, a highly discretized cutter with differentiated diameters will probably yield more accurate results. However, a reliable estimate of the pressure gradient used in this pseudo-analytical model can only be obtained through more elaborate research methods such as experiments as well as advanced computational fluid dynamics.

The calibration is based on a single cutter geometry as well as a single set of operation and hydrological parameters. In order to better calibrate the model, the model production curves should be calibrated with a wider variety of geometrical and operational parameters from different cases. Further detailing of the model parameters is recommended.

## REFERENCES

- Andrassy, C. and Herbich, J. (1988). "Generation of resuspended sediment at the cutterhead." *The Dock and Harbour Authority*, 68(797), pp. 207–216.
- Burger, M. den. (2003). "Mixture forming processes in dredge cutter heads." *Ph.D. Dissertation*, Delft University of Technology, The Netherlands.
- Becker, J., van Eekelen, E., van Wiechen, J., de Lange, W., Damsma, T., Smolders, T. and van Koningsveld, M. (2015). "Estimating source terms for far field dredge plume modelling." *Journal of Environmental Management*, 149, pp. 282-293.
- Collins, M. A. (1995). "Dredging-induced near-field resuspended sediment concentrations and source strengths." *Miscellaneous Paper D-95-2*, U.S. Army Engineer Waterways Experiment Station, Vicksburg, Miss.

- Dekker, M. A., den Burger, M., Kruyt, N. P., and Vlasblom, W. J. (2003). "Experimental and numerical investigation of cutter head dredging flows." *Journal of Waterway, Port, Coastal and Ocean Engineering*, ASCE, Vol. 129, No. 5, pp. 203-209.
- Hayes, D. (1986). "Development of a near field source strength model to predict sediment resuspension from cutter suction dredges." *MS thesis*, Mississippi State University, Mississippi State, Miss.
- Hayes, D. F., Crockett, T. R., Ward, T. J., and Averett, D. (2000). "Sediment Resuspension during Cutterhead Dredging Operations." *Journal of Waterway, Port, Coastal, and Ocean Engineering*, 126(3), pp. 153-161
- Hayes, D., McLellan, T., and Truitt, C. (1988). "Demonstrations of innovative and conventional dredging equipment at Calumet Harbor, Illinois." *Miscellaneous Paper EL-88-1*, U.S. Army Engineer Waterways Experiment Station, Vicksburg, Miss.
- Nakai, O. (1978). "Turbidity generated by dredging projects." *Proc., 3<sup>rd</sup> U.S./Japan Experts Meeting*, U.S. Army Engineer Water Resources Support Center, Ft. Belvoir, Va.
- Joanknecht L.W.F., (1976). "A review of Dredge Cutter Head Modeling & Performance." *Proceedings WODCON VII*, San Francisco, California, USA, pp. 995-1016.
- Miedema, S.A. (2017, November 11). Personal correspondence.
- Miltenburg, C.J.M. (1983). "Stroming en mengselvorming in grote snijkoppen (Flow and Mixture Forming in large cutterheads)." *Laboratoriumopdracht La0/8/101*, Laboratory of Soil Transportation, Delft University of Technology, Delft, The Netherlands. (in Dutch).
- Mol, A. (1977a). "Stroombeeld rond en in Cutter deel II: vrij in water draaiend; injecties met kleurstof (Flow around and in a cutter head part II: freely rotating in water; injections with dye)." *WL/Delft Hydraulics BAGT 236*, The Netherlands. (in Dutch).
- Moret, G.E. (1977a). "Stroombeeld rond en in Cutter deel I: Stroombeeld rondom cutter bij kunstmatige taluds; injecties met kleurstof (Flow around and in a cutter head part II: flow around cutter head placed in an artificial bank; injections with dye)." *WL/Delft Hydraulics BAGT 235*, The Netherlands. (in Dutch).
- Ngan-Tillard, D., Haan, J., Laughton, D., Mulder, A. and Nooy van der Kolff, A. (2009). "Index test for the degradation potential of carbonate sands during hydraulic transportation." *Eng. Geol.*, 108(1-2), pp. 54-64
- Nakai, O. (1978). "Turbidity generated by dredging projects." *Proc., 3<sup>rd</sup> U.S./Japan Experts Meeting*, U.S. Army Engineer Water Resources Support Center, Ft. Belvoir, Va.
- Nieuwboer, B.J. (2018, March 6). Personal correspondence.
- Slotta, L.S. (1968). "Flow visualization techniques used in dredge cutter head evaluation." *Proceedings of WODCON II 1968*, Rotterdam, The Netherlands, pp. 56-77.
- Steinbusch, P.J., Vlasblom, W.J., den Burger, M. and Kruyt, N.P. (1999). "Numerical Simulation of the Flow Generated by Cutter Heads." *Slurry Handling and Pipeline Transport*, 14<sup>th</sup> International conference, Hydrotransport 14, Maastricht, The Netherlands.
- van Rhee (2018, April 09). Personal Correspondence.
- van Rhee, C., & Bezuijen, A. (2001). "The breaching of sand investigated in large-scale model tests." *Coastal Engineering Proceedings*, 1(26).
- Vlasblom, W.J. and van Hemmen, A.J.M. (2006) "The Shape of and the Position of Teeth on a Cutter Head. The background information." *CEDA Dredging Days 2006 - Protection of the Coastline. Dredging and Sustainable Development, Tangier, Morocco*

#### CITATION

- Werkhoven, J. J., Nieuwboer, B.J., Louis, A.A., Ramsdell, R.C., and Miedema, S.A. "A pseudo-analytical model for CSD spillage due to rotational velocity-induced flow," *Proceedings of the Western Dredging Association Dredging Summit & Expo '18, Norfolk, VA, USA, June 25-28, 2018.*